DOI: https://doi.org/10.24425/amm.2025.154484

R. CHULIST<sup>©1,2\*</sup>, N. PORĘBA<sup>©1,2</sup>, W. SKROTZKI<sup>©3</sup>, A. WÓJCIK<sup>©1,2</sup>, A. SZEWCZYK<sup>©1</sup>, N. SCHELL<sup>6</sup>, A. HOHENWARTER<sup>5</sup>, R. PIPPAN<sup>5</sup>, W. MAZIARZ<sup>6</sup>

# PHASE STABILITY AND INVERSE HALL-PETCH EFFECT OF SEVERELY DEFORMED AND ANNEALED CrMnFeCoNi HIGH-ENTROPY ALLOY

The reverse phase transition from hexagonal close-packed (hcp) to face-centered cubic (fcc) was studied using diffraction of high-energy synchrotron radiation and hardness measurements on the CrMnFeCoNi high-entropy alloy deformed by high-pressure torsion (HPT) at 77 K under 10 GPa quasi-hydrostatic pressure. Cryogenic HPT leads to a nanocrystalline structure and induces a phase transition from fcc to hcp. To determine the stability of the hcp phase the material was annealed at temperatures between 473 K and 973 K for 2 h. Annealing initially results in the reverse transition to the fcc phase, followed by precipitation of body-centered cubic (bcc), fcc and then tetragonal particles. The volume fractions of particular phases over the entire temperature range were calculated using Rietveld refinement. During annealing the reverse phase transformation takes place along with grain growth and reduction in dislocation density, surprisingly leading to an increase in hardness. This phenomenon indicates an inverse Hall-Petch effect. Keywords: High-entropy alloy; microstructure; phase stability; microhardness

## 1. Introduction

The equiatomic CrMnFeCoNi high-entropy alloy (HEA), so-called Cantor alloy, is a prototype for multicomponent facecentered cubic (fcc) single-phase solid solution alloys [1-4]. It has attracted a lot of interest due to its excellent ductility and high fracture toughness [5]. The low stacking fault energy of the Cantor alloy [6,7] gives rise to massive mechanical twinning at low temperatures which accounts for the excellent combination of strength and ductility. Moreover, this alloy shows a strong temperature dependence of strength below 473 K, while it is weak at elevated temperatures. Due to a high work-hardening rate at low temperatures, large plastic stability occurs reducing the growth rate of necking. Thus, this HEA is suitable for broad applications at cryogenic temperatures [8].

By applying hydrostatic pressure at room temperature (RT), the fcc Cantor alloy is transformed into the hexagonal close-packed (hcp) structure, which is also called  $\varepsilon$ -martensite by analogy to hexaferrum ( $\varepsilon$ -Fe) [9-12]. As demonstrated in previous studies [13-16], the transformation can be driven by shear deformation and temperature, with the fraction of the ε-phase increasing with increasing hydrostatic pressure and decreasing deformation temperature. These results are consistent with ab initio calculations and show that the hcp phase is energetically favored at low temperatures [17]. In general, the hcp phase introduces an additional deformation mode in the form of phase transformation (besides slip and twinning) which improves the formability of this alloy. On the other hand, it makes the microstructure more complex, surprisingly decreasing the RT strength of the material in the nanocrystalline (nc) state [13-16]. However, there is much less consensus about the stability of the stress-induced *hcp* phase at high temperatures especially for the nc material. For example, a sample deformed at 77 K by HPT at 10 GPa and stored at RT for 1 month exhibits a volume fraction of the hcp phase of 85% [15]. After storage of this sample for two years, the volume fraction of the *hcp* phase is reduced to about 67%, which is about the level of long-term storage [15]. Structurally, it appears that storage of the severely deformed Cantor alloy containing mainly the hcp phase leads to the reconversion to the fcc phase. This can be caused by self-annealing even at RT

Corresponding author: rchulist@agh.edu.pl



INSTITUTE OF METALLURGY AND MATERIALS SCIENCE, POLISH ACADEMY OF SCIENCES, 25 REYMONTA STR., 30-059 KRAKÓW, POLAND AGH UNIVERSITY OF SCIENCE AND TECHNOLOGY, FACULTY OF METALS ENGINEERING AND INDUSTRIAL COMPUTER SCIENCE, AL. A. MICKIEWICZA 30, 30-059 KRAKOW,

TECHNISCHE UNIVERSITÄT DRESDEN. INSTITUTE OF SOLID STATE AND MATERIALS PHYSICS. D-01062 DRESDEN, GERMANY

DEPARTMENT OF MATERIALS SCIENCE, MONTANUNIVERSITÄT LEOBEN, JAHNSTRASSE 12, 8700 LEOBEN, AUSTRIA

since the HPT-deformed samples are severely deformed. It may also indicate that the hcp phase becomes unstable at ambient conditions and transforms back to the fcc phase. Therefore, the present work aims to investigate the stability of the hcp phase in a strongly deformed Cantor alloy subjected to HPT at 77 K under 10 GPa quasi-hydrostatic pressure and stored for 1 year at RT. This starting material contains a volume fraction of 68% hcp phase. To enhance the kinetics of the reverse transformation, the HPT-deformed sample was annealed for 2 h at temperatures between 473 K and 973 K. In order to gain a more comprehensive understanding of the stability of the hcp phase, the sample that was stored for only one month at RT and contains the highest volume fraction of the *hcp* phase is also included in the analysis. To distinguish this sample from the one stored for one year, it will be referred to as "77 K" because it is assumed to approximately represent the state after cryogenic deformation and pressure release. Additionally, Vickers microhardness measurements were performed to study the mechanical resistance of the annealed samples as a function of grain size and phase constitution.

# 2. Experimental details

Details of the synthesis of the equiatomic CrMnFeCoNi HEA are given in [14]. For HPT deformation, discs with a diameter of 8 mm and an initial thickness of about 0.8 mm were cut from the cast and homogenized ingots. A quasi-hydrostatic pressure of 7.8 GPa was used at 77 K to deform the sample with a speed of 0.2 rotations/min, up to 5 rotations. More details regarding the HPT process at 77 K of the Cantor alloy are provided in [18]. Since upon HPT the shear strain changes along the radius,

the samples for annealing were cut equidistant with respect to the radius to maintain a comparable magnitude of shear strain for all samples, about  $90 \pm 10$ . Annealing was done in a quartz ampoule under a vacuum of 10<sup>-5</sup> Torr. Phase analysis was performed at RT employing high-energy synchrotron diffraction in the transmission mode at beamline P07B of DESY, Hamburg, Germany, using a 2D Marview detector and High Score software [20,21]. In order to get rid of texture effects, the measurements were performed using a continuous rotation by 180° along the longest axis of the sample pin cut along the radial direction. Such a procedure allows meeting the Bragg condition for all planes and recording all reflections on one single image plate. The obtained data were reduced by integrating the intensity of each point in the 2 theta/intensity plots. It is worth mentioning that this procedure enables to receive "quasi" powder diffraction data for bulk polycrystalline samples without the need for powder milling. This significantly increases the accuracy of the calculations for Rietveld refinement. The grain size was estimated by the Scherrer equation using X-ray graphs including peak position and FWHM. For the fcc phase, the (200)<sub>fcc</sub> peak is taken since it is the only peak which does not overlap with peaks belonging to the *hcp* phase. In the case of the *hcp* phase, the (101) peak was used.

Vickers micro-hardness measurements were conducted with a Struers microhardness tester with a load of 50 gf.

## 3. Results and Discussion

Fig. 1 shows diffraction patterns taken for the Cantor alloy subjected to HPT at 77 K, stored after deformation at RT for

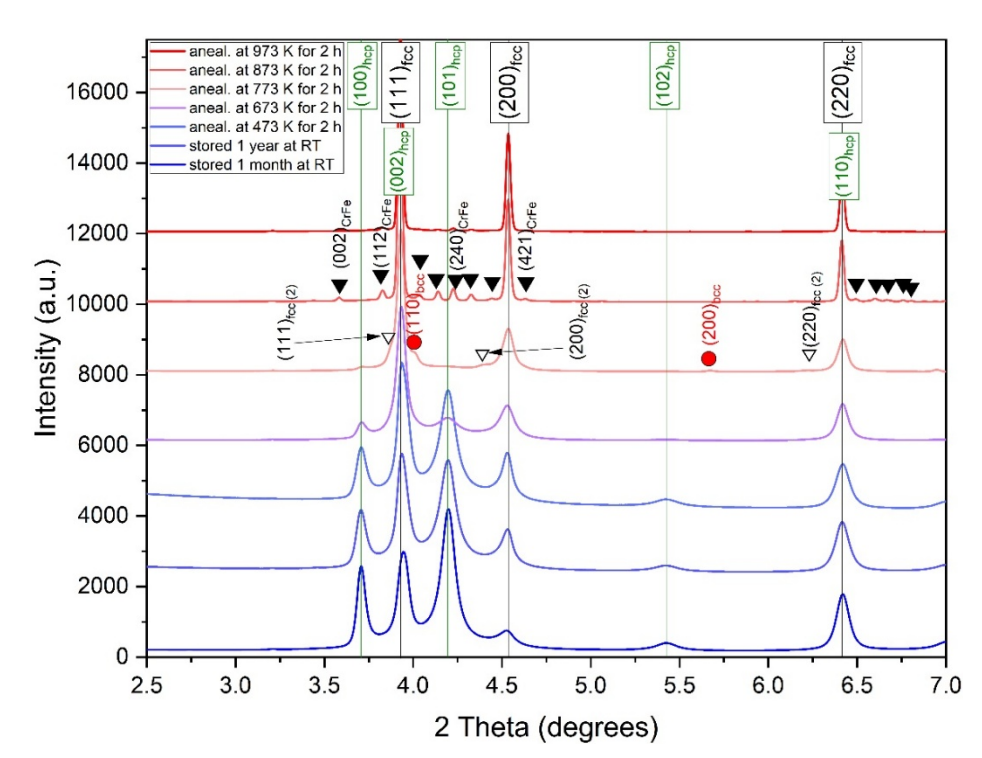


Fig. 1. X-ray diffraction patterns for the HEA sample HPT-deformed at 77 K and stored at RT for 1 month and 1 year. The latter was annealed for 2 h at different temperatures

1 month and 1 year. The latter was annealed for 2 h at higher temperatures. The sample stored at RT for one 1 year was used to check the long-term stability of the *hcp* phase at ambient temperature. Such a long time allows reaching the lower limit in terms of the volume fraction of the *hcp* phase at RT. The application of a quasi-hydrostatic pressure at 77 K transforms the HEA sample to the *hcp* phase with a volume fraction of 85%. However, storage of such a deformed sample at RT for one year leads to back transformation to *fcc*, reducing the amount of *hcp* to 68%. Raising the temperature to 473 K for 2 h, the *hcp* phase is further reduced to 49%. Eventually, the *hcp* phase disappears at 773 K and is replaced by *fcc* and body-centered cubic (*bcc*) precipitates.

Interestingly, the crystal structure of the fcc precipitates differs significantly in lattice parameter from the fcc HEA matrix indicating a different chemical composition and therefore is outlined with the number 2 in Fig. 1 for reference. At higher temperatures, a tetragonal complex CrFe-rich phase (a = 8.6283 Å, c = 4.5542 Å) precipitates with the largest tendency at 873 K [4,22-24]. As reported in [25] this structure originates from the bcc phase with almost the same composition but a different crystal structure. The phase transformations and the evolution of individual phases with regard to their volume fractions are presented in Fig. 2. As can be seen the volume fraction of the *hcp* phase decreases upon annealing for the combinations of times and temperatures chosen. The hcp phase is present up to about 673 K and thereafter the HEA decomposes into two phases, one with fcc structure and lattice parameter 3.7082 Å and the other with bcc structure and lattice parameter 2.8723 Å. At the highest temperatures, the so-called sigma phase precipitates, however, contradictory to some reports its volume fraction decreases with increasing temperature [22-25]. This effect can be related to the severely deformed material with nano grain size and can take longer in coarse-grained material [26].

The average grain size estimated by the Scherrer equation according to peak broadening for fcc and hcp phases is shown in Fig. 3. As expected the grain size of the fcc phase increases with increasing annealing temperature. Grain growth at low annealing temperatures is quite slow, with an increase in average grain size from about 30 nm at RT to about 60 nm at 673 K. Above 673 K significant grain growth takes place with an increase in the average grain size from about 60 nm to about 180 nm in the material annealed at 973 K for 2 h. It should be mentioned that only the (200) reflection for the fcc matrix was used for calculation. On the other hand, the (101) hcp peak was used to calculate the average grain size of the hcp phase. However, unlike the fcc phase, the grain size of *hcp* is rather stable showing even a small tendency to decrease with increasing annealing temperature. This effect means that part of the larger, less stable hcp nanograins were back transformed to fcc. Surprisingly, the strength of the material increases with increasing grain size of the fcc phase indicating an inverse Hall-Petch effect [27]. Fig. 4 presents the microhardness as a function of annealing temperature. The microhardness increases with grain size of the fcc phase reaching saturation at about 75 nm. Moreover, the lower the annealing temperature the larger the scatter of the microhardness which indicates a more heterogeneous microstructure within the fcc + hcp region. Yet despite the large scatter and complex microstructure incorporating a number of different precipitates, a noticeable trend can be observed for grain size softening, which is based on grain/ interphase boundary sliding. The interphase boundary sliding can also be described by the shuffle mechanism commonly observed in hcp metals [28]. An additional reason discussed for anneal-

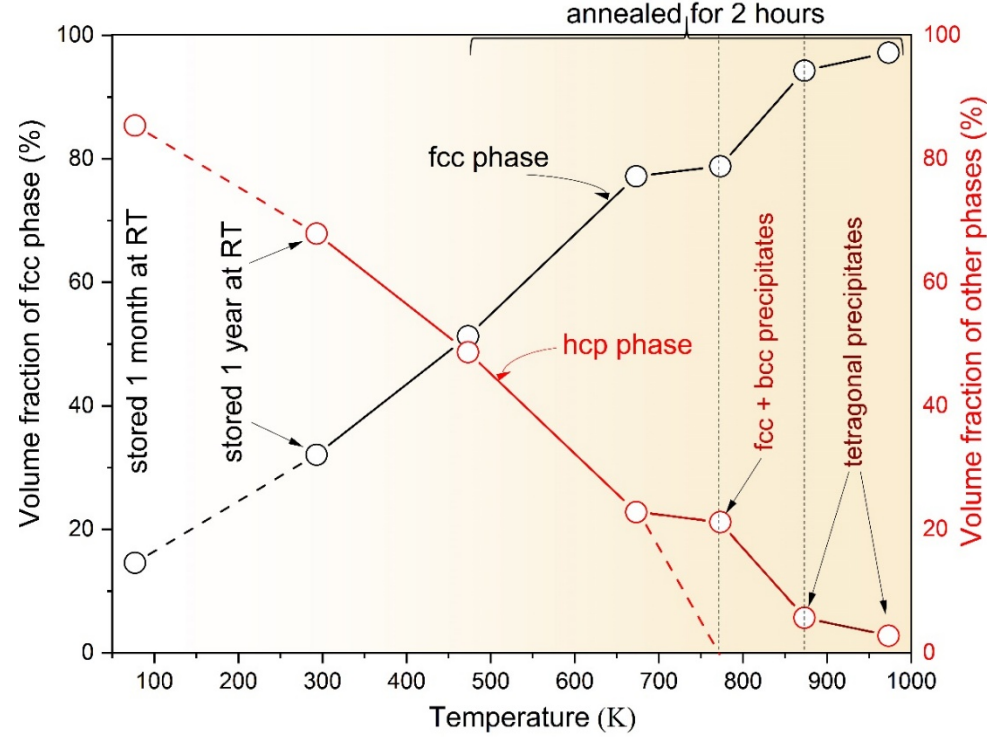


Fig. 2. Volume fraction of certain phases as a function of annealing temperature, calculated using the Rietveld refinement

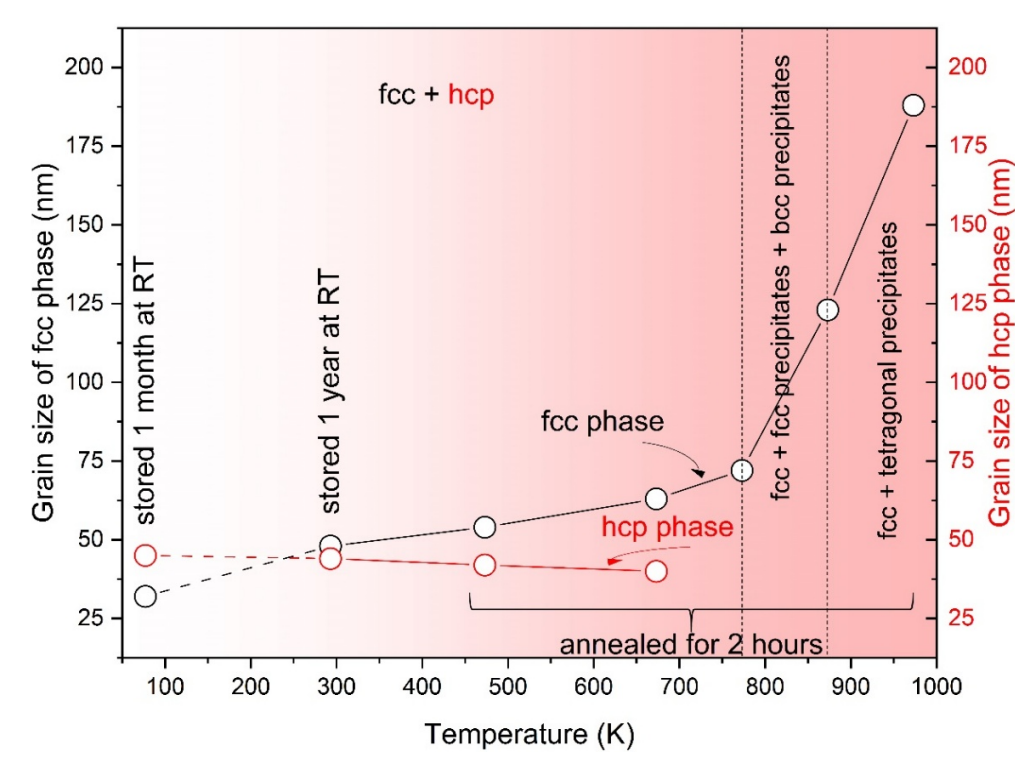


Fig. 3. Grain size of the fcc and hcp phases as a function of annealing temperature

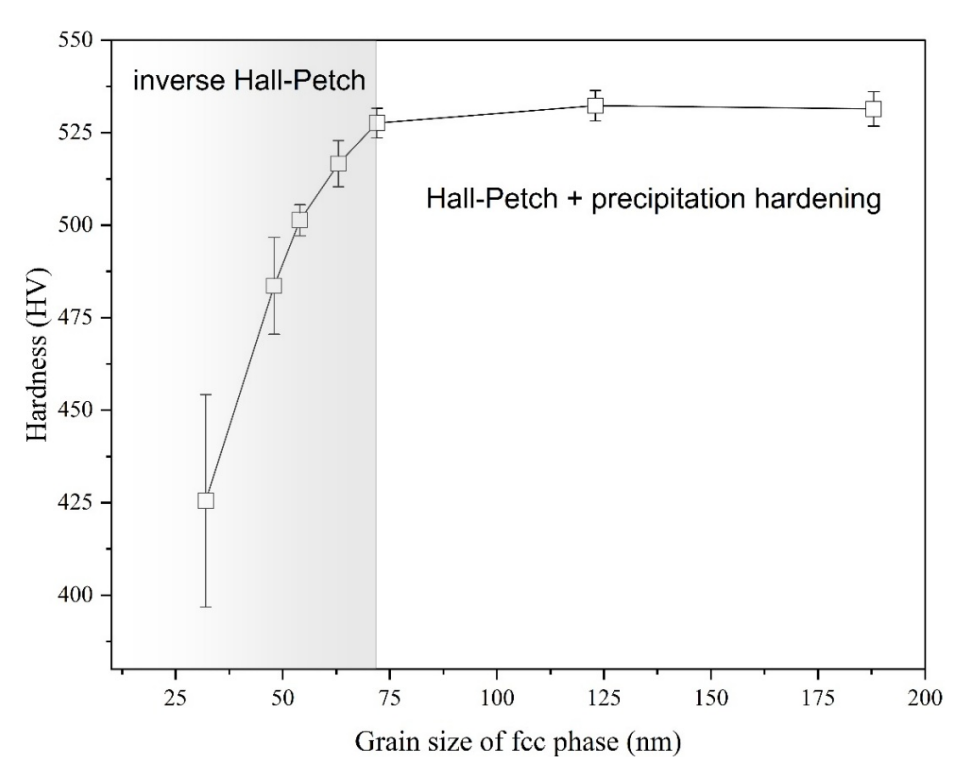


Fig. 4. Microhardness as a function of fcc grain size for a sample HPT-deformed at 77 K, stored at RT and subsequently annealed at different temperatures

hardening of nc materials is relaxation of the grain boundaries from a non-equilibrium to an equilibrium state, which makes the emission and absorption of dislocations from/in grain boundaries more difficult and therefore leads to hardening [29-31]. However, this effect can only be verified in materials where grain coarsening can be suppressed during annealing.

After exceeding 75 nm the microhardness reaches saturation even though the small particles should further increase the strength of the alloy. Thus, for grain sizes between 75 nm and 180 nm, two contrasting processes affect the strength. The first is the classic Hall-Petch effect which decreases the strength due to increasing grain size of the *fcc* phase and the second is

hardening due to *fcc*, *bcc* and tetragonal precipitates. However, to quantitatively separate the two, nanohardness measurements and TEM/EDS observations are required.

## 4. Conclusions

The phase stability of a nc CrMnFeCoNi HEA produced by HPT at cryogenic temperature was studied using diffraction of high-energy synchrotron radiation and hardness measurements. The initial HPT-deformed material exhibits a two-phase microstructure with a dominating hcp and minor fcc phase and an average grain size of about 40 and 30 nm, respectively. During annealing the reverse transformation of the hcp phase to fcc takes place. The hcp phase completely disappears at 773 K, while at above this temperature bcc, fcc and tetragonal phases begin to precipitate. The Rietveld analysis shows the development of certain phases and their volume fractions over a broad temperature range. The lower the annealing temperature the larger the scatter of the microhardness which indicates a more heterogeneous microstructure within the fcc + hcp region. This effect is not observed when small precipitations form. The estimated grain sizes along with hardness measurements indicate an inverse Hall-Petch effect based on grain/interphase boundary sliding. Interphase boundary sliding seems to be comparable or even easier than grain boundary sliding in the fcc and hcp phase. Future work will involve direct confirmation of the X-ray diffraction results through TEM/SEM observations.

## Acknowledgement

The work was financed by project No. 2020/37/B/ST5/03267 of the National Science Centre of Poland. The results were presented during 14th Polish Japanese Joint Seminar on Micro and Nano Analysis (3-6.09.2024, Toyama, Japan). The financial support of Polish Academy of Sciences is greatly appreciated.

# REFERENCES

- [1] J.W. Yeh, S.K. Chen, S.J. Lin, J.Y. Gan, T.S. Chin, T.T. Shun, C.H. Tsau, S.Y. Chang, Nanostructured high-entropy alloys with multiple principal elements: Novel alloy design concepts and outcomes. Adv. Eng. Mater. 6, 299-303 (2004). DOI: https://doi.org/10.1002/adem.200300567
- [2] B. Cantor, I.T.H. Chang, P. Knight, A.J.B. Vincent, Microstructural development in equi atomic multicomponent alloys. Mater. Sci. Eng. A 375-377, 213-218 (2004). DOI: https://doi.org/10.1016/j.msea.2003.10.257
- [3] F. Otto, Y. Yang, H. Bei, E.P. George, Relative effects of enthalpy and entropy on the phase stability of equiatomic high-entropy alloys. Acta Mater. 61, 2628-2638 (2013). DOI: https://doi.org/10.1016/j.actamat.2013.01.042

- [4] B. Schuh, F. Mendez-Martin, B. Völker, E.P. George, H. Clemens, R. Pippan, A. Hohenwarter, Mechanical properties, microstructure and thermal stability of a nanocrystalline CoCrFeMnNi highentropy alloy after severe plastic deformation. Acta Mater. 96, 258-268 (2015).
  - DOI: https://doi.org/10.1016/j.actamat.2015.06.025
- [5] E.P. George, W.A. Curtin, C.C. Tasan, High entropy alloys: A focused review of mechanical properties and deformation mechanisms. Acta Mater. 188, 435-474 (2020). DOI: https://doi.org/10.1016/j.actamat.2019.12.015
- [6] S. Huang, W. Li, S. Lu, F. Tian, J. Shen, E. Holmström, L.Vitos, Temperature dependent stacking fault energy of FeCrCoNiMn high entropy alloy. Scr. Mater. 108, 44-47 (2015). DOI: https://doi.org/10.1016/j.scriptamat.2015.05.041
- [7] M. Shih, J. Miao, M. Mills, M. Ghazisaeidi, Stacking fault energy in concentrated alloys. Nat. Commun. 12, 3590 (2021). DOI: https://doi.org/10.1038/s41467-021-23860-z
- [8] A. Gali, E.P. George, Tensile properties of high- and mediumentropy alloys. Intermetallics 39, 74-78 (2013). DOI: https://doi.org/10.1016/j.intermet.2013.03.018
- [9] N. Von Bergen, R. Boehler, Effect of non-hydrostaticity on the α-ε transition in iron. High Press. Res. 6, 133-140 (1990).
   DOI: https://doi.org/10.1080/08957959008203204
- [10] C.L. Tracy, S. Park, D.R. Rittman, S.J Zinkle, H.B. Bei, M. Lang, R.C. Ewing, W.L. Mao, High pressure synthesis of a hexagonal close-packed phase of the high-entropy alloy CrMnFeCoNi. Nat. Commun. 8, 15634 (2017). DOI: https://doi.org/10.1038/ncomms15634
- [11] F. Zhang, H. Lou, B. Cheng, Z. Zeng, Q. Zeng, High-pressure induced phase transitions in high-entropy alloys: A review. Entropy, 21, 239 (2019).
  - DOI: https://doi.org/10.3390/e21030239
- [12] F. Zhang, H. Lou, S. Chen, X. Chen, Z. Zeng, J. Yan, W. Zhao, Y. Wu, Z. Lu, Q. Zeng, Effects of non-hydrostaticity and grain size on pressure-induced phase transformation of the CoCrFeMnNi high-entropy alloy. J. Appl. Phys. 124, 115901 (2018). DOI: https://doi.org/10.1063/1.5046180
- [13] W. Skrotzki, R.Chulist, Severe plastic deformation of high-entropy alloys. Mater. Trans. 64, 1769-1763 (2023).
  DOI: https://doi.org/10.2320/matertrans.mt-mf2022050
- [14] W. Skrotzki, A. Pukenas, E. Odor, B. Joni, T. Ungar, B. Völker, A. Hohenwarter, R. Pippan, E.P. George, Microstructure, texture and strength development during high-pressure torsion of CrMn-FeCoNi high-entropy alloy. Crystals 10, 336 (2020). DOI: https://doi.org/10.3390/cryst10040336
- [15] R. Chulist, A. Pukenas, P. Chekhonin, A. Hohenwarter, R. Pippan, N. Schell, W. Skrotzki, Phase transformation in CrMnFeCoNi high-entropy alloy during high pressure torsion. Materials 15, 8407 (2022). DOI: https://doi.org/10.3390/ma15238407
- [16] K. Edalati, A.Q. Ahmed, S. Akrami, K. Ameyama, V. Aptukov, R.N. Asfandiyarov, M. Ashida, V. Astanin, A. Bachmaier, V. Beloshenko, et al. Severe plastic deformation for producing superfunctional ultrafine-grained and heterostructured materials: An interdisciplinary review. J. Alloys Compd. 1002, 174667 (2024). DOI: https://doi.org/10.1016/j.jallcom.2024.174667

- [17] D. Ma, B. Grabowski, F. Körmann, J. Neugebauer, D. Raabe, Ab initio thermodynamics of the CoCrFeMnNi high entropy alloy: Importance of entropy contributions beyond the configurational one. Acta Mater. 100, 90-97 (2015).
  - DOI: https://doi.org/10.1016/j.actamat.2015.08.050
- [18] R. Pippan, S. Scheriau, A. Hohenwarter, M. Hafok, Advantages and limitations of HPT: A review. Mater. Sci. Forum **584-586**, 16-21 (2008).
  - DOI: https://doi.org/10.4028/www.scientific.net/MSF.584-586.16
- [19] A. Wojcik, R. Chulist, P. Czaja, M. Kowalczyk, P. Zackiewicz, N. Schell, W. Maziarz, Evolution of microstructure and crystallographic texture of Ni-Mn-Ga melt-spun ribbons exhibiting 1.15% magnetic field-induced strain. Acta Mater. 219, 117237 (2021). DOI: https://doi.org/10.1016/j.actamat.2021.117237
- [20] R. Chulist, A. Wójcik, A. Sozinov, T. Tokarski, M. Faryna, N. Schell, W. Skrotzki, B. Li, H. Sehitoglu, X. Li, W. Maziarz, Adaptive phase or variant formation at the austenite/twinned martensite interface in modulated Ni–Mn–Ga martensite. Adv. Funct. Mater. 34, 2307322 (2024). DOI: https://doi.org/10.1002/adfm.202307322
- [21] F. Otto, A. Dlouhy, K.G. Pradeep, M. Kubenova, D. Raabe, G. Eggeler, E.P. George, Decomposition of the single-phase highentropy alloy CrMnFeCoNi after prolonged anneals at intermediate temperatures. Acta Mater. 112, 40-52 (2016). DOI: https://doi.org/10.1016/j.actamat.2016.04.005
- [22] E.J. Pickering, R. Munoz-Moreno, H.J. Stone, N.G. Jones, Precipitation in the equiatomic high-entropy alloy CrMnFeCoNi. Scr. Mater. 113, 106-109 (2016).
  DOI: https://doi.org/10.1016/j.scriptamat.2015.10.025
- [23] S. Schmidt, G.D. Sathiaraj, S.S. Kumar, B. Sulkowski, S. Suwas, S. Jaschinski, A. Pukenas, B. Gu, W. Skrotzki, Effect of rolling and annealing temperature on the mechanical properties of CrMnFeCoNi high-entropy alloy. Mater. Chem. Phys, 270, 124830 (2021).
  - DOI: ttps://doi.org/10.1016/j.matchemphys.2021.124830

- [24] F. Zhang, Y.Wu, H.B. Lou, Z.D. Zeng, V.B. Prakapenka, E. Greenberg, J.Y. Yan, J.S.; Okasinski, X.J. Liu, Y. Liu, et al. Polymorphism in a high-entropy alloy. Nat. Commun. 8, 15687 (2017). DOI: https://doi.org/10.1038/ncomms15687
- [25] M-H. Tsai, H. Yuan, G. Cheng, W. Xu, W.W. Jian, M.-H. Chuang, C.-C. Juan A. Yeh S.J. Lin, Y. Zhu, Signicant hardening due to formation of sigma phase matrix in a high entropy alloy. Intermetallics 33, 81-86 (2013).
  - DOI: https://doi.org/10.1016/j.intermet.2012.09.022
- [26] G. Laplanche, S. Berglund, C. Reinhart, A. Kostka, F. Foxa, E.P. George, Phase stability and kinetics of σ-phase precipitation in CrMnFeCoNi high-entropy alloys. Acta Mater. 161, 338-351 (2018).
  - DOI: https://doi.org/10.1016/j.actamat.2018.09.040
- [27] S.N. Naik, S.M. Walley, The Hall-Petch and inverse Hall-Petch relations and the hardness of nanocrystalline metals. J. Mater. Sci. 55, 2661-2681 (2020).
  - $DOI: \ https://doi.org/10.1007/s10853-019-04160-w$
- [28] B. Li, X.Y. Zhang, Twinning with zero twinning shear, Scr. Mater.
   125, 73-79 (2016).
   DOI: https://doi.org/10.1016/j.actamat.2018.07.027
- [29] O. Renk, A. Hohenwarter, K. Eder, K.S. Kormout, J.M. Cernay, R. Pippan, Increasing the strength of nanocrystalline steels by annealing: Is segregation necessary? Scr. Mater. 95, 27-30 (2015).
- [30] J. Gubicza, Annealing-induced hardening in ultrafine-grained and nanocrystalline material Adv. Eng. Mater. 22, 1900507 (2020). DOI https://doi.org/10.1002/adem.201900507

DOI: https://doi.org/10.1016/j.scriptamat.2014.09.023

- [31] O. Renk, A. Hohenwarter, V. Maier-Kiener, R. Pippan, Exploring the anneal hardening phenomenon in nanocrystalline PtRu alloys. J. Alloys Compd. 935, 168005 (2022).
  - DOI: https://doi.org/10.1016/j.jallcom.2022.168005